Available online at www.sciencedirect.com
ScienceDirect
Physica E 40 (2008) 1044–1047
PHYSICA E
www.elsevier.com/locate/physe

Time-resolved interference experiments in a solid state environment

S. Gustavsson[a,*], R. Leturcq[a], M. Studer[a], T. Ihn[a], K. Ensslin[a], D.C. Driscoll[b], A.C. Gossard[b]

[a]*Solid State Physics Laboratory, ETH Zurich, CH-8093 Zurich, Switzerland*
[b]*Materials Department, University of California, Santa Barbara, CA 93106, USA*

Available online 8 January 2008

Abstract

We investigate interference of electrons in an Aharonov–Bohm geometry with two embedded quantum dots. The interfering electrons are detected using time-resolved charge detection methods. The Aharonov–Bohm oscillations have a visibility higher than 90%, demonstrating a high degree of phase coherence in the system. We use the technique to probe phase shifts for excited states in one of the embedded quantum dot.

PACS: 73.21.La; 73.23.−b

Keywords: Aharonov–Bohm; Interference; Quantum dots; Single-electron detection

The Aharonov–Bohm (AB) effect provides one of the best examples of quantum mechanical phase-coherence [1]. Electrons passing the two arms of a ring acquire a phase difference due to the magnetic flux enclosed by the two paths. As a result, the outgoing current shows oscillations as a function of applied magnetic field. The effect has been observed in both metallic [2] and semiconductor [3] rings, as well as in carbon nanotubes [4]. The AB effect has also been used as a tool for investigating coherent transport of other devices. Measurements of the transmission phase of a quantum dot (QD) were demonstrated by embedding the QD into one arm of an AB ring [5–7].

Here, we report on measurements of interference of individual electrons in an AB geometry (see Fig. 1(a)). The structure consists of two QDs in series (marked by 1 and 2) coupled via two separate tunneling barriers, formed in the left and right arms between the QDs. Electrons enter the structure from the source lead, go through QD1 and pass on to QD2 through the two arms. Upon arriving in QD2, the electrons are counted one-by-one using time-resolved charge detector techniques. Apart from measuring interference of individual electrons, we use the setup to investigate the transmission phase of excited states in one of the QDs [8].

The sample was fabricated using scanning probe lithography [9] on a $GaAs/Al_{0.3}Ga_{0.7}As$ heterostructure with a two-dimensional electron gas (2DEG) 34 nm below the surface. The quantum point contact (QPC) used as a charge detector is seen in the upper-right corner of the figure. The gates T, B, L and R are used to tune the height of the tunneling barriers, while gates G1 and G2 control the electrochemical potentials of the two QDs. In the experiment, we tune the tunnel barriers between source and QD1 (Γ_S) and between drain and QD2 (Γ_D) to a few kHz. This is essential to ensure reliable detection of individual electrons with the finite-bandwidth detector [10]. On the other hand, the coupling t between the QDs is kept at larger values, typically a few GHz. All measurements were performed in a dilution refrigerator with an electronic temperature of 60 mK.

The conductance of the QPC is strongly influenced by the electron population of the QDs [11]. By voltage biasing the QPC and continuously monitoring its conductance, electrons transport in the QDs can be detected in real-time [12–14]. In Fig. 1(b), we plot two typical time traces of the QPC conductance, showing a few electrons entering and leaving the QDs. The traces were taken with no bias applied to the double QD (DQD), so that the tunneling is

*Corresponding author.
E-mail address: simongus@phys.ethz.ch (S. Gustavsson).

1386-9477/$ - see front matter © 2007 Elsevier B.V. All rights reserved.
doi:10.1016/j.physe.2007.09.209

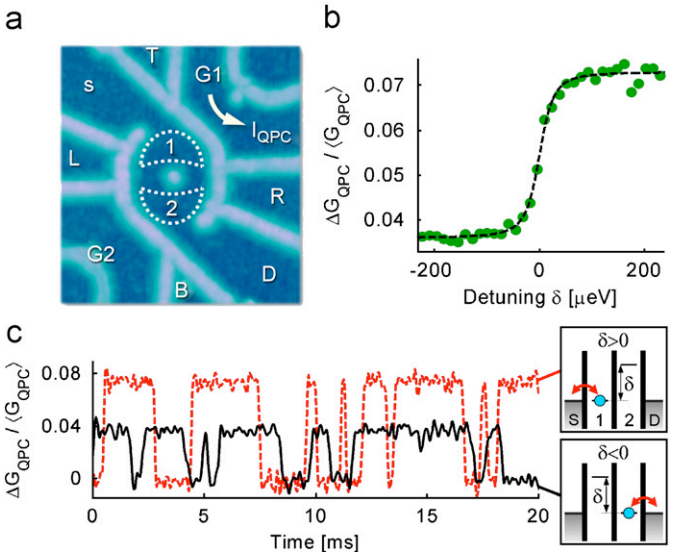

Fig. 1. (Color online) (a) Sample used in the experiment. The structure consists of two QDs (marked by 1 and 2), connected by two separate paths. The conductance of the nearby quantum point contact (QPC) is used to read out the charge state of the QDs. (b) Time-resolved measurement of the QPC conductance, showing a few electrons entering and leaving the QDs. Since the QPC is located closer to QD1, an electron tunneling in QD1 gives a larger signal than an electron tunneling in QD2. (c) Average population of QD1, $p_1/(p_1+p_2)$, measured as a function of detuning δ between the two QDs. The dashed line is the theoretical expectation from a tunnel-coupled two-level system, with coupling energy $t = 14\,\mu\text{eV}$.

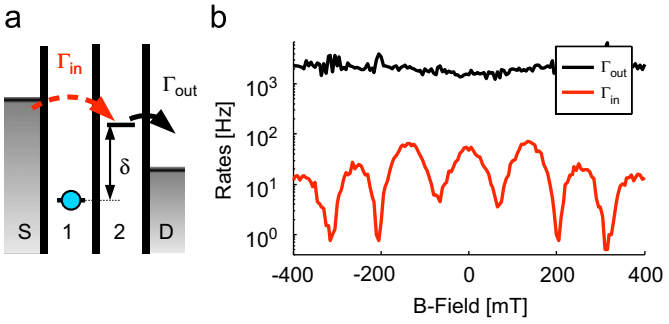

Fig. 2. (Color online) (a) Schematic drawing of the QD energy levels in the cotunneling configuration. QD1 is detuned by an energy δ relative to QD2. Sequential tunneling is suppressed, but electrons may still tunnel from source into QD2 by means of a virtual process. (b) Tunneling rates Γ_{in} and Γ_{out} measured versus applied magnetic field. The rate Γ_{in} corresponds to electrons cotunneling through QD1 and passing the two arms of the ring before arriving in QD2. The partial waves passing the two paths pick up a phase difference due to the magnetic flux enclosed between them, giving rise to strong AB oscillations. On the other hand, Γ_{out} stays constant within the region of interest.

due to equilibrium fluctuations between either source and QD1 (dashed curve) or between drain and QD2 (solid line). Analyzing traces such as the one shown in Fig. 1(b), the rates for electron tunneling into and out of the QD can determined separately [13,15].

Since the QPC is located closer to QD1 than QD2, the QPC conductance is more strongly influenced by electron tunneling in QD1. For the data shown in Fig. 1(b), the detuning δ between the electrochemical potential of QD1 and QD2 is large compared to the tunnel coupling t between the two QDs. Here, the electrons are well described by states residing completely on either QD1 or QD2. In Fig. 1(c), we plot the change in QPC conductance for one electron leaving the DQD as a function of δ. For $\delta \ll -t$, the electron is mainly residing in QD2, giving a small ΔG_{QPC}. In the opposite limit, $\delta \gg t$ and the electron is mainly sitting in QD1, so that ΔG_{QPC} is larger. When $|\delta| \sim t$, the states in the QDs hybridize and form a molecular state distributed over both QDs. In this case, ΔG_{QPC} gives a direct measurement of the charge localization in the DQD. The dashed line in Fig. 1(c) is the fit expected for a tunnel-coupled two-level system [16], giving a coupling $t = 3.4\,\text{GHz} = 14\,\mu\text{eV}$. The results of Fig. 1(b)–(c) show that we have a well-defined double dot system. The combination of time-resolved charge detection methods and charge localization measurements allow the couplings of the system to be precisely determined.

Next, we apply a bias $V_{bias} = 600\,\mu\text{V}$ to the DQD and put the electrochemical potential of QD1 outside the bias window, as depicted in Fig. 2(a). In this configuration, the electron in QD1 lacks an energy δ needed for leaving to QD2 and we expect sequential transport to be suppressed. Still, electrons may cotunnel directly from source to QD2 by means of a virtual process. Due to the time-energy uncertainty principle, there is a time window of length $t \sim \hbar/\delta$ where tunneling from QD1 to QD2 followed by tunneling from source to QD1 is possible.

Coming back to the picture of the sample in Fig. 1(a), we see that there are two separate paths available for the cotunneling process; the electron may go through either the left or the right arm when passing from QD1 to QD2. If the process is phase-coherent, we expect partial waves passing the two paths to interfere upon arriving in QD2. By applying a magnetic field perpendicular to the sample, we introduce a phase difference between the two paths [1]. We thus expect the cotunneling rate to show an oscillating behavior with magnetic field.

Fig. 2(b) shows a measurement of Γ_{in} and Γ_{out} versus magnetic field. Since electrons can only enter the DQD through the cotunneling process and only leave by tunneling from QD2 to the drain, we can directly identify $\Gamma_{in} = \Gamma_{cot}$ and $\Gamma_{out} = \Gamma_D$. The cotunneling rate does indeed show strong AB-oscillations, with an oscillation period $\Delta B = 130\,\text{mT}$ corresponding well to one flux quantum $\Phi = h/e$ penetrating the loop formed by the two arms connecting the QDs. The visibility of the AB-oscillations is above 90%, demonstrating the high degree of phase coherence in the system.

The rate for electrons leaving the DQD (Γ_{out}) shows almost no variations with the applied magnetic field. This is expected, since the electrons leave the DQD by direct tunneling from QD2 to drain. This process does not involve any interfering paths. It can also be noted that for

the whole measurement range, we have $\Gamma_{in} \ll \Gamma_{out}$. This demonstrates the low probability of the cotunneling process.

In the following, we investigate the phase of the AB-oscillations for different states of QD2. Previous experiments have shown phase shifts of π occurring between consecutive Coulomb resonances in many-electron QDs [5,6]. To measure AB-oscillations for consecutive electron fillings requires a relatively large shift of the gate voltages. Such measurements are difficult to perform in our setup, since large changes of gate voltages also affect the symmetry of the left and right arm connecting QD1 and QD2, which may strongly reduce the visibility of the AB-oscillations. Instead, we look at excited states of QD2 at fixed electron population [8].

Depending on the direction of the applied bias, different excited states are probed. Fig. 3 shows the energy level diagrams of the system for different bias directions, including an excited state in QD2. The typical level spacing in QD2 is $\Delta E \sim 200\,\mu eV$, as determined from finite bias spectroscopy [17]. For positive bias, electrons cotunnel from source into QD2 and may thereby put QD2 into either its GS (GS) or first excited state (ES^+). The transition involving the excited state requires the incoming electron to supply an extra energy ΔE. For negative bias (Fig. 3(b)), the cotunneling involves an electron leaving QD2. The QD is left in either its GS or in an excited state. Here, the transition involving the excited state (ES^-) occurs at an energy ΔE *below* the GS transition.

After some time, the excited QD will relax to its GS. However, this occurs on a timescale of $\sim$1 ns [18], which is much longer than the time available for cotunneling, $\hbar/\delta \sim 10$ ps. Therefore, we expect the measured cotunneling rate to be independent of relaxation. This allows us to use the cotunneling rate as a probe of the AB phase of the excited state.

We first focus on the situation with negative bias applied to the QDs (Fig. 3(b)). Fig. 4(a) shows a measurement of the electron count rate versus magnetic field and total energy ε of the DQD system relative to the leads. The detuning δ is kept fixed during the whole measurement. We

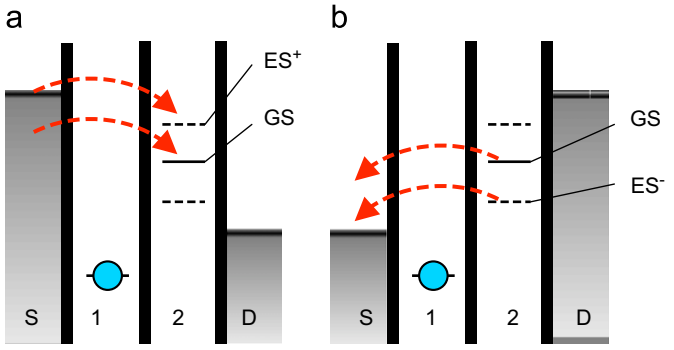

Fig. 3. (Color online) (a) Energy level diagram for positive bias. The cotunneling probe the GS and the ES^- excited state. (b) Same for negative bias. Here, the GS and the ES^--state are involved in the cotunneling process.

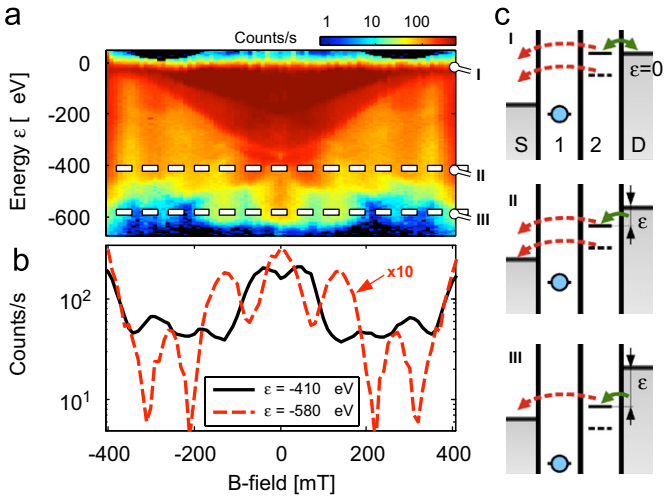

Fig. 4. (Color online) (a) Electron count rate, measured versus magnetic field and total energy of the DQD relative to the leads, ε. (b) Count rates measured at the positions marked by the dashed lines in (a). There is a phase shift of 0.7π between the two curves. The trace for $\varepsilon = -580\,\mu eV$ has been magnified by a factor of 10 for better visibility. (c) Energy diagrams of the DQD for the positions marked by I, II and III in (a). At point I, the potential of QD2 is lined up with the Fermi level in the right lead and the tunneling is mainly due to equilibrium fluctuations between QD2 and the lead. At point II, the DQD potential is shifted downwards, so that electrons in QD2 may only leave by cotunneling to the left lead. The energy level arrangement allow a process involving an excited states of QD2 to contribute to the cotunneling. Finally, at point III only cotunneling involving the GS of QD2 is possible.

define $\varepsilon = 0$ when the potential of QD2 is aligned with the Fermi level of the drain lead (see case I in (c)). Here, the tunneling is mainly due to equilibrium fluctuations between QD2 and the drain. As ε is reduced, the equilibrium fluctuations between QD2 and drain are no longer possible and electrons can only leave QD2 by cotunneling to the source. This process involves interfering paths and the count rate in Fig. 4(a) show clear AB-oscillations. Between the dashed lines marked by II and III, both the intensity and the behavior of the count rate changes drastically. Fig. 4(b) shows two cross section from Fig. 4(a), taken at the positions of the dashed lines. Both traces show AB-oscillations, and both curves are symmetric around $B = 0\,T$ as expected from the Onsager relations. However, by comparing the positions of the maxima for $B > 0\,T$ we see that the phase is shifted by 0.7π between the two curves.

Starting at point III in Fig. 4(a)–(c), the state ES^- is below the Fermi level of the source so that only cotunneling through the GS is possible. The trace in Fig. 4(b) belonging to point III is qualitatively similar to the one shown in Fig. 2(b), with both curves having a maximum appearing at $B = 0\,T$. The similarity is expected, since both measurements involve cotunneling through the GS of QD2. Moving to point II, the energy of the DQD is shifted upward so that also the excited state may contribute to transport. The cotunneling rate measured in this regime is a sum of the processes involving the GS and the excited state. However, since the rates at point II are almost an

order of magnitude larger compared to point III, the behavior is to a large extent dominated by cotunneling from the excited state.

From this, we conclude that there is a phase shift of 0.7π between the AB signal involving the GS and the ES^- excited state of QD2. Similar measurements were done for the ES^+ state involved in cotunneling at positive bias. Although the excited state is clearly visible as an overall increase in the cotunneling rate, for this configuration we do not see any phase shift compared to the GS AB signal (not shown). Our findings are in agreement with previously reported results [5,6,8], but more measurements are needed to map out the complete phase behavior of the QD spectrum.

To conclude, we have measured interference of individual electrons tunneling through an AB ring. With visibility of more than 90%, we demonstrate a high degree of coherence in the system. In addition, we use the technique to probe the transmission phase of excited states in one of the QDs embedded in the ring.

References

[1] Y. Aharonov, D. Bohm, Phys. Rev. 115 (1959) 485.
[2] R.A. Webb, et al., Phys. Rev. Lett. 54 (1985) 2696.
[3] G. Timp, et al., Phys. Rev. Lett. 58 (1987) 2814.
[4] A. Bachtold, et al., Nature 397 (1999) 673.
[5] R. Schuster, et al., Nature 385 (1997) 417.
[6] M. Avinun-Kalish, et al., Nature 436 (2005) 529.
[7] M. Sigrist, et al., Phys. Rev. Lett. 96 (2006) 036804.
[8] M. Sigrist, et al., Phys. Rev. Lett. 98 (2007) 036805.
[9] A. Fuhrer, et al., Superlattices Microstruct. 31 (2002) 19.
[10] O. Naaman, J. Aumentado, Phys. Rev. Lett. 96 (2006) 100201.
[11] M. Field, et al., Phys. Rev. Lett. 70 (1993) 1311.
[12] L.M.K. Vandersypen, et al., Appl. Phys. Lett. 85 (2004) 4394.
[13] R. Schleser, et al., Appl. Phys. Lett. 85 (2004) 2005.
[14] T. Fujisawa, et al., Appl. Phys. Lett. 84 (2004) 2343.
[15] S. Gustavsson, et al., Phys. Rev. Lett. 96 (2006) 076605.
[16] L. DiCarlo, et al., Phys. Rev. Lett. 92 (2004) 226801.
[17] W.G. van der Wiel, et al., Rev. Mod. Phys. 75 (2002) 1.
[18] T. Fujisawa, et al., Nature 419 (2002) 278.